JOURNAL OF Materials Feature Article CHEMISTRY

Silica encapsulation of quantum dots and metal clusters

P. Mulvaney,*[a] L. M. Liz-Marzán,[b] M. Giersig[c] and T. Ung[a]

[a]*School of Chemistry, University of Melbourne, Parkville, VIC., 3052, Australia. E-mail: p.mulvaney@chemistry.unimelb.edu.au*
[b]*Depto de Química Física, Universidade de Vigo, E-36200 Vigo, Spain*
[c]*Hahn-Meitner Institut, Berlin, Glienickerstr. 100, 14109, Germany*

Received 16th December 1999, Accepted 19th January 2000
Published on the Web 13th April 2000

The use of nanometre thick silica shells as a means to stabilize metal clusters and semiconductor particles is discussed, and its potential advantages over conventional organic capping agents are presented. Shell deposition depends on control of the double layer potential, and requires priming of the core particle surface. Chemical reactions are possible within the core, *via* diffusion of reactants through the shell layer. Quantum dots can be stabilized against photochemical degradation through silica deposition, whilst retaining strong fluorescence quantum yields and their size dependent optical properties. Ordered 3D and 2D arrays of a macroscopic size with uniform particle spacing can be created. Thin colloid films can also be created with well-defined interparticle spacing, allowing controlled coupling of exciton and surface plasmon modes to be investigated. A number of future core–shell nanocomposite structures are postulated, including quantum bubbles and single electron capacitors based on Au@SiO_2.

Introduction

Colloid chemists have traditionally neglected the solid state properties of the particles they stabilize. For example, DLVO theory[1] dispenses with the particle properties through the macroscopic Hamaker constant. Nevertheless, very often it is the solid-state properties of the colloid particles that make them of interest. For example the manganese oxides employed in alkaline batteries, the TiO_2 powders used as photocatalysts, the doped ZnO and ZnS powders incorporated into cathode-ray screens as phosphors, and the silver halide particles employed in photographic film all owe their enormous importance to their particular solid state properties. This neglect of the solid state is partially due to lack of control. Colloid chemists have great difficulty in controlling many important particle parameters such as crystal structure, crystal shape and habit, electrical conductivity, doping levels and surface state energies. However, the increasing need for rigorous control over the optical, fluorescent and conductive properties of wet-chemically prepared nanoparticle systems has refocussed colloid research of the last ten years onto the solid state properties of colloids and the associated issue of particle nucleation. At stake are revolutions in the design of economic single electron transistors and quantum dot circuitry,[2] subpicosecond NLO switching devices and quantum dot lasers,[3] efficient solar cells,[4] photocatalysts for pollutant removal[5] and new methods for immunolabelling.[6]

With the advent of new scanning probe microscopies, atomic resolution TEM, single particle electron diffraction and single particle elemental analysis, it has now become feasible to design and build particles with a focus on the solid state architecture and the particle band structure rather than just on the overall particle stability. Of course ultimately, the particles so synthesized must be stable against coalescence, which can obliterate size-dependent optical features, and the designers of more complicated structures must exploit both conventional double-layer interactions and other system specific interactions such as steric and hydration forces, as a means to engineer more complicated structures.

A fundamental problem is that nanoparticle technologies usually involve the preparation of metallic, magnetic and semiconducting particles in a wide variety of matrices including zeolites,[7] Langmuir–Blodgett films,[8–10] organic solvents,[11–13] inverse micelles,[14–16] polymers,[17–19] glasses,[20–23] sol–gel derived thin films,[24–27] and water.[28–32] In many practical cases, the particles may be required in the final form as dry, redispersible powders.[33–36] The usual technique is to precipitate the particles *in situ*, directly within the matrix of interest. However, this requires new preparation procedures to be developed for each medium. All the effort that has previously been expended optimizing the preparation of a particular material in a different medium is completely squandered through this procedure. For example, methods for preparing highly fluorescent, almost monodisperse CdS[29] and CdSe particles[11] have been developed in water and trioctylphosphine oxide respectively. If these particles were of some utility in a glass matrix, it would seem advantageous to make these particles in the ''optimized'' solvent, and then to transfer them to the vitreous matrix, rather than to carry out laborious, time-consuming experimentation restudying their nucleation and growth kinetics within the glass. To obviate these matrix effects, a generic capping procedure is needed which fulfils the following requirements: (1) optical transparency, (2) chemical inertness, (3) photochemical stability even under laser photolysis, (4) cheapness, (5) colloidal stability at high volume fractions, (6) easy transfer into a wide range of media, and (7) simple coating methodology. Silica coating is one possible solution to these prerequisites, and in this article we examine some of the properties of silica coated nanoparticles.

I.A Double layer stabilization of small particles

When any colloid is nucleated, it faces several possible fates—redissolution, ripening, coagulation or stabilisation. The greatest practical challenge is to prevent coagulation. Even in the absence of van der Waals interactions, Brownian encounters are frequent enough to cause aggregation of nanoparticle sols within a few seconds. For instance, gold sols formed by citrate reduction typically contain approximately 10 nM particles of around 15 nm diameter. The diffusion limited rate constant for particle encounters in such a system is about 10^{11} M^{-1} s^{-1}. Hence each particle undergoes about 1000 encounters with other particles each second. To prevent rapid and irreversible coalescence and consequent loss of all size-dependent features, the particles must be stabilised. In aqueous solution, electrostatic stabilisation is the most commonly utilised method. For two small colloid particles of radius R, less than about 10 nm in size in a simple $z:z$, dilute

aqueous electrolyte, the double layer interaction is given approximately by:[37,38]

$$V/kT = 2\pi\varepsilon_r\varepsilon_o R\psi_o^2 \exp(-\kappa H) - AR/12H \quad (1)$$

where H is the surface separation, A the composite Hamaker constant, ψ_o the electric potential at the particle surface, and κ is the diffuse layer screening parameter, which is given by

$$\kappa^2 = 2z^2F^2c_o/\varepsilon_r\varepsilon_o RT \quad (2)$$

Here, c_o refers to the concentration of $z:z$ electrolyte in the solvent, and $\varepsilon_r\varepsilon_o$ is the permittivity of the medium. It is seen that both the repulsive and attractive interactions scale with the particle radius. This has two important consequences for nascent colloid systems. Firstly, for smaller sizes, a larger ψ_o is required to obtain the same repulsive interaction energy, and secondly, the secondary minimum will deepen as the particles grow or aggregate. Thus nanoparticles coalesce more readily, but repeptisation from the secondary minimum is also easier than for larger agglomerates. Phase diagrams for a variety of conditions are given in an article by Wiese and Healy,[39] but they restricted themselves to particles larger than about 50 nm. In Fig. 1, we show calculated particle interaction curves for 10 Å and 100 Å radius particles using eqn. (1). In colloid chemistry, it is conventional to take 5–10 kT as the necessary barrier for reasonable colloid stability.[40] As is immediately clear from Fig. 1, the smaller particles do not generate sufficient repulsion for colloid stability and coalescence will be reasonably rapid. For the larger particles, we note the barrier to coalescence is now very large, and in addition a secondary minimum forms, which means colloid particles will experience weak flocculation forces. (To distinguish between weak aggregation due to the secondary minimum, the term "flocculation" is often used. Such particles can be repeptised. Conversely, "coagulation" refers to particles that have attained the primary minimum. In normal DLVO (Derjaguin–Landau–Verwey–Overbeek) systems,[37] such particles cannot repeptise, and coalescence is irreversible.) Wiese and Healy also pointed out that the critical coagulation concentration of electrolyte needed to induce particle aggregation decreases rapidly as the particle size decreases because of the smaller electrostatic repulsion.[39] Nanoparticles are particularly susceptible to coalescence and "salting out" but as they aggregate, or ripen and grow, the repulsive interaction energy between aggregates or particles strengthens, and the aggregates "self-stabilize" against coagulation into the primary minimum. These trends have been explored by Miller and Zukoski in a recent review.[41]

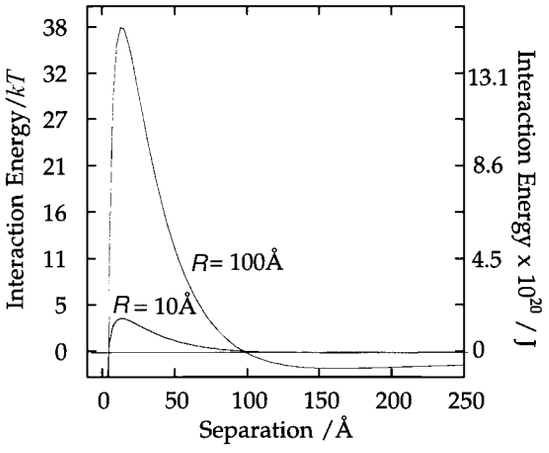

Fig. 1 Interaction curves for two gold particles using a low κa approximation [eqn. (1)], with values of $A = 2 \times 10^{-19}$ J, $\psi_o = 0.1$ V, $\kappa^{-1} = 30$ Å for $R = 10$ Å and $R = 100$ Å.

I.B AFM Measurements and nanoparticle stability

The major difficulty with most capping agents is that they are too short to mask the van der Waals interaction. As pointed out by Israelachvili, for two surfaces (1), with adsorbed layers (2), interacting across a medium (3), *i.e.* a so-called 1 : 2 : 3 : 2 : 1 system, the Hamaker function is still dominated by the substrate interactions, *i.e.* the 1 : 3 : 1 Hamaker function.[42] The adsorbed layers do not contribute significantly until the intersurface separation is less than the adsorbed layer thickness, which for a typical surfactant layer will be no more than about 1.5 nm, and substantially less for adsorbed ions. Only capping agents able to induce short-range, repulsive solvent interactions or which can create steric or osmotic repulsive forces will function well. The problem is that, in general, direct measurements of the double layer properties of nanoparticles are quite difficult. Conventional measurements of the particle electrophoretic mobility require optical detection of the particle, and even for light scattering systems employing laser doppler detection, only materials which scatter strongly, such as silver and gold, are easily measured or highly concentrated, monodisperse nanoparticle systems, which are rarely achievable in practice. Yet, information on the way adsorbates, capping agents and designer ligands modify particle and solvent interactions with particles is fundamental to improved nanoparticle formulations. Before examining the properties of silica coated nanoparticles, we consider how both silica coating and a typical organic stabiliser modify the surface chemistry of gold sols, a typical nanoparticle employed in a number of optical and biological applications.

To quantify the double layer properties we use AFM to directly measure the forces between a micron-sized gold sphere and a gold plate. AFM measurements allow direct quantification of the forces between naked or capped surfaces.[43–46] The AFM measures changes in the forces between two surfaces, usually between a sphere and a flat plate, and for exact values, the sphere must be of a known radius, and extremely smooth. Placement onto AFM microcantilevers by optical microscopy restricts the practical particle radius to 1–5 μm. The measured force is the negative gradient of the interaction energy, and for a sphere–plate system, the deflection due to van der Waals forces obeys:

$$F = -AR/6H^2 \quad (3)$$

where F is the force determined from the deflection of the cantilever *via* Hooke's Law, and H is the separation between

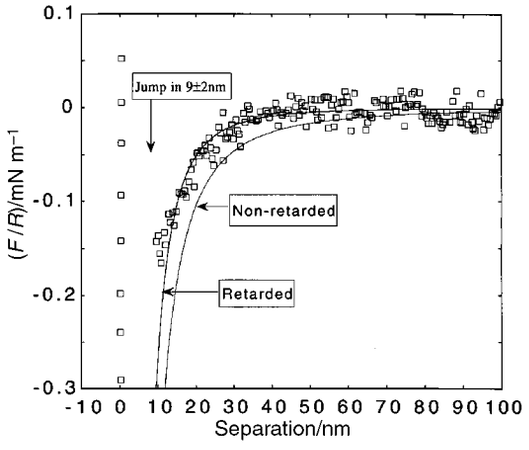

Fig. 2 Measured AFM interaction between a clean gold sphere and an evaporated gold film.[46] Both surfaces were cleaned with $H_2SO_4 : H_2O_2$ to remove organic contamination prior to measurement, and displayed zero contact angles at the start of experiments. The fitted curves are for both non-retarded and retarded Hamaker functions.[37] Reprinted with permission from *J. Chem. Phys.*, 1994, **100**, 8501.

surfaces. In Fig. 2, we show double layer forces between two gold surfaces in water. A strong attractive interaction is seen which can be fitted to a value of $A = 2.5 \times 10^{-19}$ J.[47] This is consistent with Lifschitz theory, which yields values of (1.0–4.1) $\times 10^{-19}$ J, depending on the source of the dielectric data,[47] but is much higher than that determined by Enüstün and Turkevich, on the basis of coagulation studies.[48] To offset the van der Waals forces responsible for particle coalescence, carboxylic acids are often employed to generate a negative surface charge density. These may be humic acids, tannic acids or simpler acids such as ascorbic and citric acids. Self-assembled carboxylic acids ensure dense coating of the gold surface. In the presence of a self-assembled monolayer of $HS(CH_2)_{10}COOH$, a repulsive interaction is seen, as shown in Fig. 3, where interaction curves are presented as a function of solution pH at a fixed electrolyte concentration of 0.1 mM.[49,50] The data have been fitted using DLVO theory with the surface potential as an adjustable parameter; the decay length is determined by the ionic strength of the electrolyte through the Debye screening length, eqn. (2). At shorter distances, there is a jump into contact, due to the van der Waals interaction, as predicted. At higher pH values, the ionization of the surface carboxyl groups *via*:

$$Au-S(CH_2)_{10}COOH \rightleftharpoons Au-S(CH_2)_{10}COO^- + H^+ \quad (4)$$

leads to increased surface potentials, as expected. However, the surface potential is very sensitive to added salt. The addition of salt has two effects as shown in Fig. 4, where the pH has been fixed, and electrolyte has been added. Firstly, the Debye screening length decreases, as expected from eqn. (2). Secondly, the surface potential decreases; however, the decrease is much greater than expected from simple diffuse layer theory. The decrease can be accounted for if Na^+ binding reduces the number of ionized carboxyl groups, *via* eqn. (5).

$$Au-S(CH_2)_{10}COO^- + Na^+ \rightleftharpoons Au-S(CH_2)_{10}COONa \quad (5)$$

This binding limits the build up of potential at high pH to values < -80 mV. Above 10 mM $NaNO_3$, the potential drops below -30 mV which is usually considered to mark the transition from a stable to an unstable colloid.

The AFM data allow us to understand some of the properties of the traditional Turkevich gold sols more comprehensively than in the past. Thus, nanoparticles of gold or other materials stabilized by ionizable carboxyl groups are likely to coagulate at higher salt concentrations. This sensitivity to high salt concentrations drastically reduces the ease of scale-up and processing of nanoparticles stabilized by

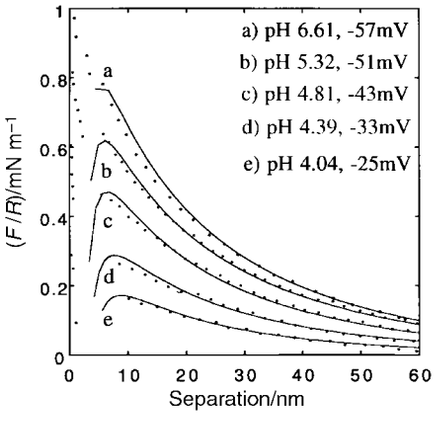

Fig. 3 Effect of pH on the interaction between a gold sphere and plate derivatized with $HSC_{10}H_{20}COOH$.[50] There is increased repulsion at higher pH values as the surface carboxyl groups become ionised. At small separations, the surfaces jump into contact due to van der Waals interactions. Reprinted with permission from *Langmuir*, 1998, **14**, 3303, copyright 1998, American Chemical Society.

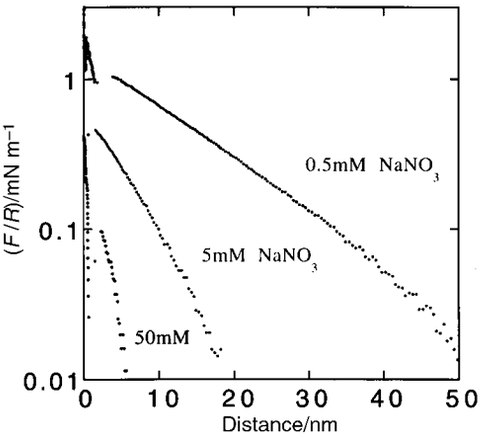

Fig. 4 The effect of added $NaNO_3$ at pH 6.0 on the interaction curve between a gold sphere and a gold plate derivatized with $HSC_{10}H_{20}COOH$.[50] The range of the repulsive interaction decreases when electrolyte is added, but the surface potential also decreases strongly due to sodium ion binding to the surface. Reprinted with permission from *Langmuir*, 1998, **14**, 3303, copyright 1998, American Chemical Society.

this sort of head group, at least in water, unless the ionic strength can be kept extremely low. Similar interaction forces have been observed between gold surfaces with adsorbed citrate ions, a common stabilizer for metal nanoparticles.[44] Whilst one may question the validity of applying such macroscopic data to nanoparticle double layers, there can be little doubt that the AFM allows one to "see" the effects of adsorbates on surface interactions, and provides important insights into nanoparticle stability. Crucially, most colloids stabilised through electrostatic repulsion are very sensitive to salt and counter ion neutralisation. Such colloids are difficult to prepare as concentrated sols, and cannot usually be easily transferred into less polar media.

I.C Silica double layer interactions

Silica behaves anomalously in water. Firstly, it does not coalesce at its isoelectric point around pH 2, as predicted by DLVO theory.[51–56] Secondly, it shows strong stability at near neutral pH at high salt concentrations.[51–56] These two features are explicable in terms of strong, short-range hydration or Stern layer forces. It is generally believed that there are hydrogen bonded layers of water adjacent to the surface, which modify the water network at the surface, and provide steric repulsion. In addition, adsorption of strongly solvated cations to the negative surface sites is also supposed to modify the solvent structure. The range of these forces is about 4 nm in the case of silica, and they are sufficiently strong to reduce or completely mask the dispersion interaction at higher surface potentials. Such a colloid can be indefinitely stable, even at high volume fractions, because the added salt actually assists particle stabilization. It is also likely that solubility equilibrium involves the formation of polymeric silicates,[51,52] which spend time in dynamic adsorption equilibrium with the parent surface, and which create a large steric layer. Direct evidence for the existence and importance of these short range forces has been gleaned from both AFM and SFA measurements using quartz surfaces and silica particles.[38,56] In Fig. 5 and 6 we show AFM interaction data for a fresh silica sphere coming into contact with a silica plate, as a function of both pH and electrolyte concentration. Again, the long distance decay obeys the usual diffuse layer predictions of DLVO theory (or Debye–Hückel equations), but at short ranges, the jump into contact disappears and repulsion is seen all the way into contact of the two surfaces.

The obvious advantages of a silica surface over normal

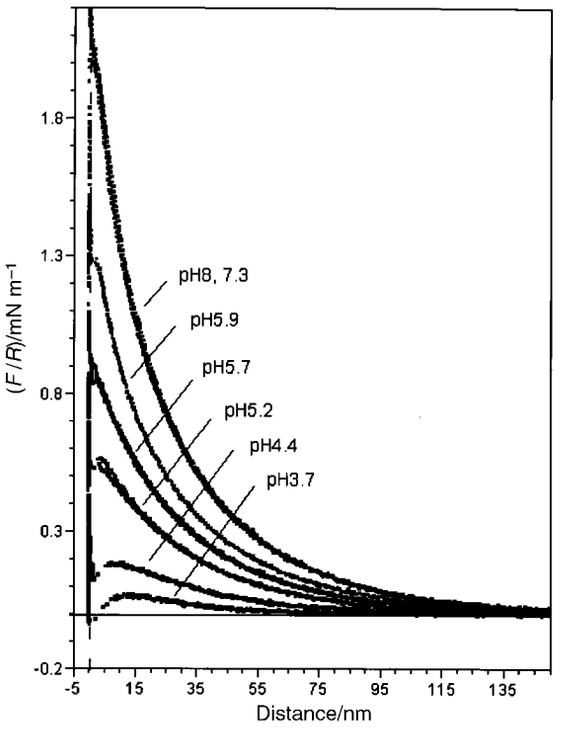

Fig. 5 AFM force curves obtained from the interaction between a silica sphere and a silica plate as a function of pH at fixed ionic strength.[56] Reprinted from *Langmuir*, 1997, **13**, 2207, copyright 1997, American Chemical Society.

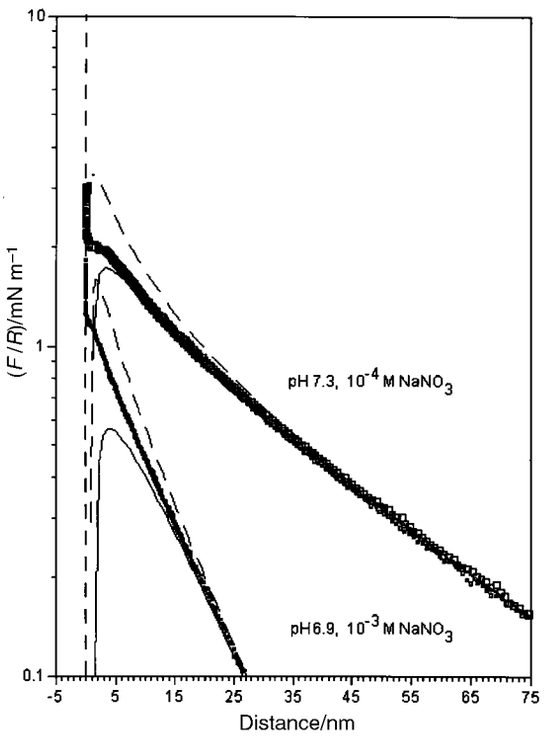

Fig. 6 AFM force curves obtained from the interaction between a silica sphere and plate as a function of ionic strength at pH 6 obtained for the interaction.[56] Reprinted from *Langmuir*, 1997, **13**, 2207, copyright 1997, American Chemical Society.

ionogenic double layer formation are that the coated particle is stable at high volume fractions and can endure large variations in pH and electrolyte concentration without coalescing, an essential prerequisite for commercial process development. Finally, the colloids are stable at higher temperatures which is important for applications involving laser irradiation of nanoparticles.[57] High volume fractions of $X@SiO_2$ nanoparticles can be rendered hydrophobic by silanization processes, so that the final particles may be incorporated into glasses, polymers, films or non-polar solvents. We conclude this section by listing in Table 1 some of the hydrophobing agents used to modify silica particles. This list is derived from the extensive work of Vrij *et al.*,[58,59] and Ford and coworkers.[60]

Table 1 Hydrophobing agents for silica particles

Silanating agent	Reference
3-(Trimethoxysilyl)propyl methacrylate (TPM) $CH_2{=}C(CH_3)COO(CH_2)_3Si(OCH_3)_3$	58
Stearyl alcohol $HS(C_3H_7)Si(OCH_3)_3$	58
Mercaptopropyltrimethoxysilane	59
$CH_2OCH–C_3H_7–Si(OCH_3)_3$, 3-Glycidoxypropyltrimethoxysilane	59
$NH_2–C_3H_7–Si(OCH_3)_3$ Aminopropyltrimethoxysilane	60
Octadecanol	60
Octadecyltrimethoxysilane	60

I.D Deposition of silica onto vitreophobic surfaces

Deposition of a coating onto a colloid surface is not straightforward, and requires a clear understanding of the double layer properties of the material being coated, since the deposition must of necessity destroy the existing stabilizing layer of ions, charges or molecules at the surface. Yet, simultaneously, coalescence must be minimized. The preceding sections have canvassed some key double layer attributes that need to be considered. Firstly, since most sols are negatively charged, silicate adsorption is electrostatically unfavourable. Furthermore, adsorption is generally only favoured on metal oxide surfaces.[61] Organic or metal surfaces are not receptive, and good nucleation is difficult and irreproducible. Initial attempts at silica deposition using standard Stöber methods were not very successful.[62] The key step is to activate the colloid surface through a silane coupling agent.[63] The key molecules are the commercially available $HSC_3H_6Si(OR)_3$ (or MPS) and $NH_2C_3H_6Si(OR)_3$ (or APS) where R = methoxy, ethoxy. These molecules have a strong chemical affinity for metal surfaces through the terminal amine or mercaptan moieties but the siloxy group will convert the surface into a vitreophilic one. Two prerequisites are that the surface not already be stabilized by covalently linked adsorbates, and that the colloid be negatively charged. The double layer potential must remain negative during adsorption of the activator. Addition of APS actually causes the electrophoretic mobility of the citrate stabilized particle to become more negative as shown in Fig. 7,[64] due to ionisation of the acidic silanol groups. As a result, citrate coated surfaces can be efficaciously activated towards silica, which means that a variety of colloids can be coated with silica *via* APS activation if the colloid can be initially synthesized using citrate ions as stabilisers. A further possible simplification in the preparation of silane stabilized particles has been demonstrated by Pastoriza-Santos and Liz-Marzán, who showed that reduction of silver salts in *N*,*N*-dimethylformamide in the presence of APS led directly to silane coated nanoparticles.[65]

II.A Basic optical properties of nanoparticles

A key reason for constructing materials out of nanoparticles is their size-dependent optical properties. In the following, we review briefly the absorption of light by nanoparticles, as a basis for understanding the perturbations introduced by deposition of silica.

The extinction spectrum of a dilute solution of small spheres

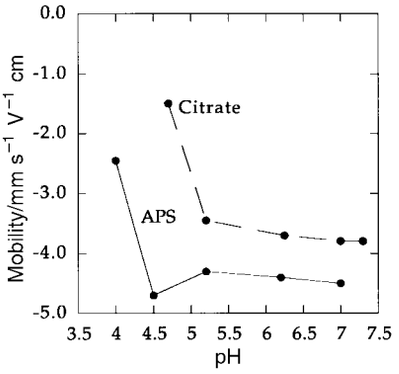

Fig. 7 Electrophoretic mobility of citrate stabilized gold sols before and after addition of APS. Data collected using laser doppler electrophoresis.

in a medium of dielectric function ε_m is given by:[66]

$$E(\mathrm{M}^{-1}\ \mathrm{cm}^{-1}) = \frac{Q_{ext} 3\times 10^{-3} V_m}{9.212R} \quad (6)$$

with R the cluster radius in cm, V_m the metal molar volume (10.43 cm^3 mol^{-1} for Au), and Q_{ext} the extinction cross-section of a single particle. The actual absorption of light by the solution, a process which results in conversion of light into heat, is described by eqn. (7). Light scattering makes a contribution of only a few percent for particles under 10 nm in diameter.[67]

$$Q_{ext} \approx Q_{abs} = \frac{18\pi\varepsilon_m^{3/2}}{\lambda} = \frac{\varepsilon''_c}{(\varepsilon'_c + 2\varepsilon_m)^2 + \varepsilon''^2_c} \quad (7)$$

The consequences of eqn. (7) have been extensively explored for the case of small metal particles, but much less so for semiconducting or insulating particles. For metals, the UV-visible response to light is usually dominated by the free electrons in the conduction band. The confinement of the conduction electrons to a small sphere causes the plasmon oscillations to become restricted to a small frequency range usually located in the visible or ultraviolet part of the spectrum. Colloidal metals are transparent at longer wavelengths in the IR region, unlike bulk metals which absorb strongly. The resonance condition for maximum excitation of the surface plasmon is given by

$$\varepsilon'_c = -2\varepsilon_m \quad (8)$$

provided that damping is small. Taking the metal to have the simple dielectric function

$$\varepsilon'_c = \varepsilon_\infty - \lambda^2/\lambda_p^2 \quad (9)$$

the peak position obeys

$$\lambda^2_{peak} = \lambda_p^2(\varepsilon_\infty + 2\varepsilon_m) \quad (10)$$

Here ε_∞ is the high frequency value of the dielectric function (about 4.9 for silver and 13.2 for gold), and λ_p is the metal's bulk plasma wavelength, given by

$$\lambda_p^2 = 4\pi^2 c^2 m\varepsilon_o / Ne^2 \quad (11)$$

The value for ε_∞ is determined by all the transitions within the metal at UV and higher frequencies. In eqn. (11), N is the electron concentration, m the effective mass of the conduction electrons and ε_o is the vacuum permittivity. As is clear from eqn. (10), the peak position is sensitive to ε_m, the solvent dielectric constant ($\varepsilon_m = 1.78$ for water), and to changes in λ_p. The primary parameter of importance in λ_p is N. Changes to the particle charge density alter the plasma frequency and can cause a shift in band position. Likewise immersion of particles or films into solvents of varying refractive index will alter their spectra, as pointed out explicitly by Shklareskii and coworkers, and verified quantitatively for metal particle films by Papavassiliou and by Underwood and Mulvaney for gold sols.[68–70]

In Fig. 8, the basic response of "naked" metal particles is shown.[71] The figure shows a plot of the real part of the dielectric function, eqn. (9), for two metals with different values of λ_p, but keeping ε_∞ constant with a value of 1. The conditions for surface plasmon resonance are given by the intersection of the dispersion curves with the horizontal solvent lines. The solvent dielectric function usually varies only weakly with wavelength. If the solvent is initially ε_{m1} , then the surface plasmon band for metal 1 will be at position A. If the solvent refractive index increases to ε_{m2}, the band will shift to the new intersection point C. Conversely, metal 2 will have a band at B that shifts to intersection point D with an increase in solvent polarizability. Most metals have values of λ_p in the UV, between 100 and 250 nm, a value determined primarily by the fact that the electron concentrations are fairly similar in metals. The dielectric function becomes negative at wavelengths longer than λ_p, and this is necessary for resonance as given by eqn. (8). As we see from the dispersion curves, by shifting to a higher electron concentration, the surface plasmon band is shifted to shorter wavelengths.

If alloying of the two metals, 1 and 2, shown in Fig. 8 is possible, the alloy tends to have a dielectric function intermediate between the two curves of the pure metals, due to the average electron concentration being determined by the mole fractions of each component. Thus alloying of 1 and 2 in a solvent of index ε_{m1} will cause the plasmon band to move along the line AB in the simplest case.[72–76]

II.B Basic optical properties of core–shell particles

The construction of nanostructured materials based on X@SiO_2 particles also requires some consideration of the optical effects of the shell. One primary effect is a weakening of the plasmon band sensitivity to solvent refractive index changes. For the nanometre sized objects considered here, the particles may still be accurately treated as dipole oscillators. In this case the extinction cross-section can be calculated from electrostatics to be[77]

$$Q_{ext} = 4x\mathrm{Im}\left[\frac{(\varepsilon_s-\varepsilon_m)(\varepsilon_c+2\varepsilon_s)+(1-g)(\varepsilon_c-\varepsilon_s)(\varepsilon_m+2\varepsilon_s)}{(\varepsilon_s+2\varepsilon_m)(\varepsilon_c+2\varepsilon_s)+(1-g)(\varepsilon_s-2\varepsilon_m)(\varepsilon_c-\varepsilon_s)}\right] \quad (12)$$

where x is given by

$$x = 2\pi R\varepsilon_m^{1/2}/\lambda \quad (13)$$

and the subscript c refers to the core and s to the shell material, and g is the volume fraction of the shell layer. The radius R refers to the coated particle radius. Note that ε_c is a complex function, while ε_s and ε_m are real. That is, we assume a dispersionless and non-absorbing medium, ε_m, and ε_s is the dispersionless dielectric function of the shell, which for the calculations on silica deposition is taken to be $\varepsilon_s = n_s^2 = 2.25$. The molar extinction coefficient of the colloid is still given by

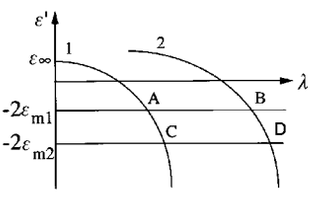

Fig. 8 Dispersion diagram showing the conditions for surface plasmon absorption as a function of the wavelength of the incident light.[71]

eqn. (6). The existence of the shell layer modifies the condition for plasmon oscillations. Surface plasmon modes occur in the composite particle when the denominator of eqn. (12) is zero, *i.e.* when

$$\varepsilon'_c = -2\varepsilon_s \frac{\varepsilon_s g + \varepsilon_m(3-g)}{\varepsilon_s(3-2g) + 2\varepsilon_m g} \quad (14)$$

For thin shells, $g \ll 1$ and the condition for resonance becomes:

$$\varepsilon'_c = -2\varepsilon_m \frac{2g(\varepsilon_s - \varepsilon_m)}{3} \quad (15)$$

This reduces to the usual resonance condition for small spheres in the absence of a coating as $g \rightarrow 0$, *i.e.* to eqn. (8). Looking first at metals, we see that if the dielectric function obeys eqn. (9), then upon insertion into eqn. (15) the peak position is determined by:

$$\frac{\lambda^2_{peak}}{\lambda^2_p} = \varepsilon_\infty + 2\varepsilon_m + \frac{2g(\varepsilon_s - \varepsilon_m)}{3} \quad (16)$$

A plot of λ^2_{peak} *versus* ε_m will now have a slope less than 2. This is due to the fact that the shell layer is polarized by light too, and sets up a dipole which may augment the core polarization charge, causing a red-shift, or it may act to reduce the core polarization giving a blue-shift compared to the uncoated particle resonance position. In the limit of very thick shells, $g \rightarrow 1$, and the surface plasmon band becomes insensitive to the existence of the medium. The particles "resonate" as though immersed in a solvent made of the shell material. This is most readily apparent if we consider the decreasing core volume fraction, f. Since $f = 1-g$ and $f \ll 1$, we can rewrite the resonance condition as:

$$\varepsilon'_c = -2\varepsilon_s \frac{\varepsilon_s(1-f) + \varepsilon_m(2+f)}{\varepsilon_s(1+f) + 2\varepsilon_m(1-f)} \quad (17)$$

For small f, this reduces to:

$$\varepsilon'_c = -2\varepsilon_s \frac{(\varepsilon_s + 2\varepsilon_m) + f(\varepsilon_m - \varepsilon_s)}{\varepsilon_s + 2\varepsilon_m} \quad (18)$$

As $f \rightarrow 0$, the plasmon resonance shifts towards a limiting value of $\varepsilon_c = -2\varepsilon_s$, *i.e.* the core sees only the shell layer as the surrounding medium, and the surface plasmon peak position is given by

$$\frac{\lambda^2_{peak}}{\lambda^2_p} = \varepsilon_\infty + 2\varepsilon_s \left[\frac{(\varepsilon_s + 2\varepsilon_m) + f(\varepsilon_m - \varepsilon_s)}{\varepsilon_s + 2\varepsilon_m}\right] \quad (19)$$

For typical values of $\varepsilon_s = 2.25$, and for $\varepsilon_m = 1.7$ to 3, and with $f = 0.05$, a plot of λ^2_{peak} *versus* ε_m will have a slope less than 0.1, *i.e.* the surface plasmon mode will be frozen at the value of $\varepsilon_c = -2\varepsilon_s$, and show no sensitivity to solvent refractive index changes. The damping effect of silica deposition on the solvent sensitivity is summarized in Fig. 9, where the ratio $\lambda^2_{peak}/\lambda^2_p$ is plotted *versus* ε_m, using eqn. (19).

The effects of the solvent refractive index on the colour of *uncoated* gold sols have been reported elsewhere.[70] Clear colour changes can be seen by eye even for changes as small as $\Delta n = \pm 0.01$. Conversely, for silica coated particles, changing the refractive index from 1.36 to 1.50 results in only minute changes in position. A comparison of the observed shifts for uncoated particles and for the same particles when coated with 10 nm of silica is shown in Fig. 10.[70,78] The uncoated particles show a monotonic increase in peak position with increasing refractive index. The effect is drastically reduced for the 10 nm coated particles.

For spherical semiconductor and insulating particles, eqn. (6), (7) and (12) also describe the optical absorption spectrum. But, in general, there is no simple analogue to the Drude model of the metal dielectric function for semiconductor particles. Furthermore, the onset of quantum size effects for quite large particles means that there are deviations from bulk dielectric behaviour for most materials of interest. Consequently, there has been less use of simple dielectric theory to interpret the optical absorption spectra of quantum dots in solution.

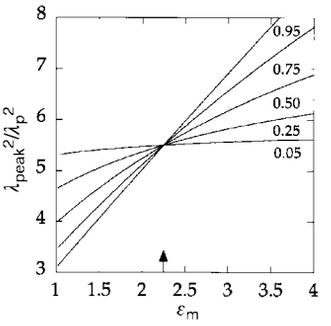

Fig. 9 Position of the normalized surface plasmon band position ($\lambda^2_{peak}/\lambda^2_p$) as a function of the medium refractive index for different shell volume fractions. Increasing shell volume fraction, g, decreases the sensitivity to solvent changes. The calculations assume the metal to have a simple Drude dielectric function and $\varepsilon_s = 2.25$.

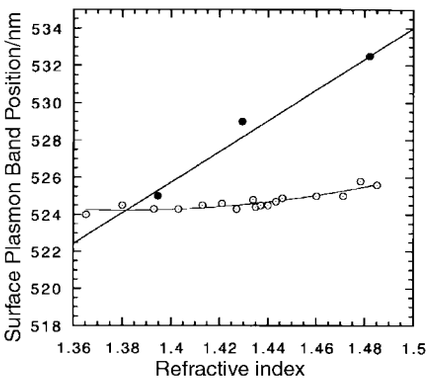

Fig. 10 Shift in the peak position for uncoated 15 nm diameter gold sols as a function of the solvent refractive index (dark circles[70]), and for silica coated gold sols with a 10 nm shell (open circles[78]) and $\varepsilon_s = 2.25$.

II.C Index matching, surface plasmon shifts and exciton shifts

The degree of scattering by the shell layer can be controlled by altering the solvent refractive index. This means that even if the particles are grown to micron size by silica deposition, the sol can still display the optical properties of the nanoparticle core. To index match silica coated particles where the shell has a refractive index, $n_s = 1.456$, the particles can be dispersed in ethanol–toluene mixtures, after derivatizing the Au@SiO_2 with TPM.[78] The effect is shown in Fig. 11. The sol in ethanol is turbid pink, but deepens to a transparent red as the solvent refractive index is raised from 1.36 to 1.46. The experimental and calculated spectra are shown as a function of refractive index in Fig. 12.

For both coated and uncoated semiconductor particles, the solvent refractive index has only a small effect on the position of the exciton band. Calculated spectra for AgI colloids are shown in Fig. 13. The exciton band is red-shifted only 1–2 nm on raising the solvent refractive index from 1.3 to 2.0.[71] This system was chosen because good dielectric data are available for the spectral region near the onset of interband transitions and also for the dielectric response of excitons within the crystal. The exciton absorption behaves almost exactly as a simple harmonic oscillator superimposed onto the dielectric response of the interband transitions.[79] Because of the large

Fig. 11 Photograph of $Au@SiO_2$ colloids (15 nm core diameter and 83 nm shell thickness) as a function of the mixed toluene–ethanol refractive index. The refractive index varies from 1.36 for the sample on the right to 1.456 for the far left sample.[85] Reprinted from *Langmuir*, 1996, **12**, 4329, copyright 1996, American Chemical Society.

positive contribution to $\varepsilon(\lambda)$ from lattice polarization, the value of ε' is always positive, and this reduces the role of "Mie resonances" [eqn. (8)] in determining the position of the exciton band. Quantum size effects are far more dramatic than solvent effects in determining exciton shifts; the exciton in Q-AgI is located at about 330 nm for a size of 3.5 nm, compared to a bulk value of 420 nm.[80] Index matching is only of importance for larger colloids of insulators and semiconducting materials as a means to reduce light scattering.

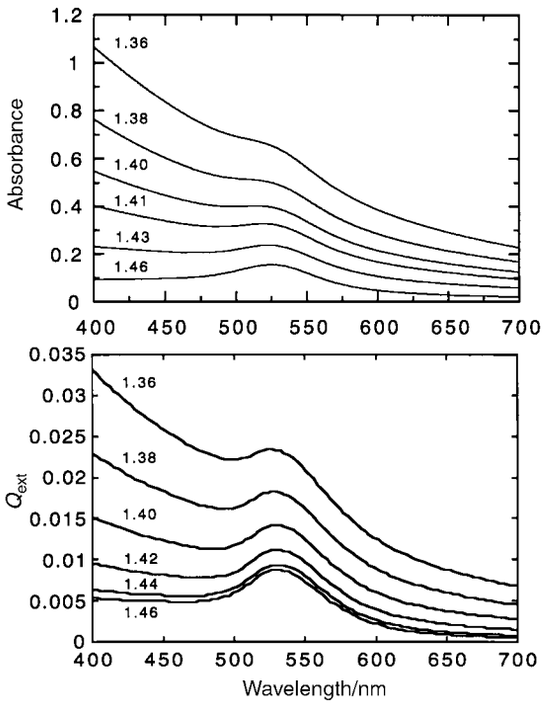

Fig. 12 Experimental (above) and calculated spectra (below) of $Au@SiO_2$ colloids (15 nm core, 83 nm shell) *versus* solvent refractive index.[78] Reprinted from *Langmuir*, 1996, **12**, 4329, copyright 1996, American Chemical Society.

II.D Concentrated nanoparticle systems and films

In the previous sections, we have noted that for metal particles, changes in solvent refractive index and the deposition of silica lead to pronounced changes to the absorption spectrum, effects which are barely discernible for quantum dots. Likewise, when $X@SiO_2$ particles condense to form films, the optical perturbations are much stronger for metal cores than for semiconductors. $Au@SiO_2$ crystallizes to form ordered arrays with brilliant colours ranging from red, purple, blue and green depending on the interparticle spacing, which is controlled by the silica shell.[81] For thick shells, the crystals remain blood red, and may appear golden or green or red in reflected light. For thinner shells, the conduction electrons interact and the plasmon band red-shifts.[81] The absorption spectra of two such films are shown in Fig. 14 and colour images are presented in Fig. 15. There are numerous models to account for the dipole interaction between the gold colloid particles, which cause these colour shifts. These "effective" medium models date back to Maxwell-Garnett and Bruggemann.[82,83] Granqvist and Hunderi have previously examined dense gold clusters[84] deposited from vacuum, but their island films consisted of very heterogeneous particles, and were rarely spherical. Moreover, the interparticle spacing varied considerably within the films. $Au@SiO_2$ crystals more closely approximate a model system for these theories. The coupling is most simply treated using Maxwell-Garnett theory

$$\varepsilon_{av} = \varepsilon_m * (1 + a/b) \tag{21}$$

where

$$a = \frac{3f(\varepsilon - \varepsilon_m)}{\varepsilon + 2\varepsilon_m} \tag{22}$$

$$b = 1 - \frac{f(\varepsilon - \varepsilon_m)}{\varepsilon + 2\varepsilon_m} \tag{23}$$

Here f is the volume fraction of the core particles in the matrix. The volume-average refractive index n_{av} and absorption coefficient k_{av} of the composite material can be extracted from eqn. (21)–(23), and inserted into the slab equations for thin films to calculate the absorption spectra of $Au@SiO_2$ nanoparticulate films. The coupling can be controlled through the silica shell thickness. Whilst a more complete description will be given elsewhere,[85] we present here some images of such films to illustrate how the silica volume fraction has been utilized to modulate the particle dipole coupling and hence the film colour.

The quality of the films is due to the homogeneous packing dictated by the uniform particle size and shell thickness. These films have been self-assembled from a single colloid using

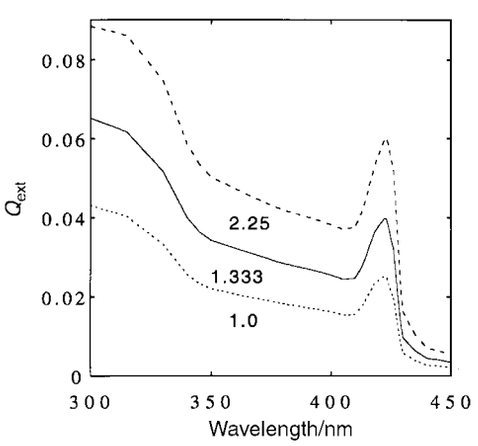

Fig. 13 Calculated extinction spectra of 5 nm radius AgI spheres as a function of the solvent refractive index. Dielectric data from ref. 79.

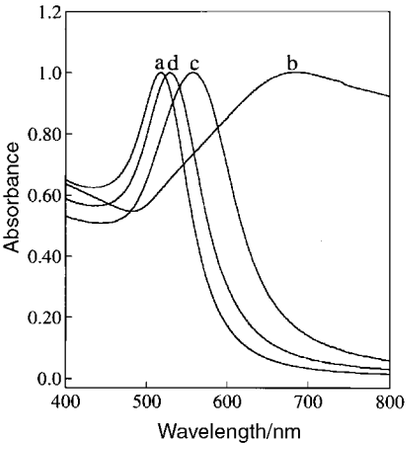

Fig. 14 Spectra of dense $Au@SiO_2$ films as a function of the gold volume fraction.[71] Particle core has diameter 15 nm.[85] Silica shell thickness: *a* 17.5, *b* 0.5, *c* 1.5, *d* 4.6 nm.

cationic polymers as an interlayer glue, a technique pioneered by Fendler and coworkers.[86] Each film is prepared after different periods of deposition from a silicate solution. As the shell thickness decreases, the coupling increases, causing, through eqn. (21)–(23), a deepening of the colour to crimson and then purple. For the thinnest shells, ≈ 3 nm thick, the colour is close to blue, the colour of conventional evaporated gold films. When the silica shell thickness is >12 nm, the particles do not interact, and the film is transparent and homogeneously red.

Fig. 15 Photographs of dense $Au@SiO_2$ films with 15 nm diameter core gold particles, and different shell thicknesses. The top left film is a sputter coated gold film. The next two bluish films are formed from gold sols which have sodium citrate (0.5 nm) and sodium mercapto-propionate (1.0 nm) shells, the other films utilise gold colloids with silica shells having thickesses: 1.5 nm, 2.9 nm, 4.6 nm, 12.2 nm and 17.5 nm. The shell thickness controls the dipole coupling between particles and hence the colour of the film. The homogeneous particle size ensures homogeneous film colour. For shells greater than about 15 nm in thickness, the particles are almost completely isolated, and the transmitted colour is similar to that of the colloid. As the shell thickness is reduced, the colour shifts from red to crimson to purple and finally for 0.5–1 nm thick shells to a blue colour similar to that found for conventional evaporated gold films. The reflected colour also changes gradually from a green tinge through to a metallic gold colour as the coupling increases.

These film images exemplify the marvellous opportunities nanoparticle optics offer for the design of unique materials, with properties tunable from nanoparticle to bulk optical behaviour, in this case simply through modulation of the diluent film matrix. In fact, such optical effects are inevitable in any high volume fraction nanoparticle film, no matter how small the individual particles. In the case of exciton absorption in quantum dots, red-shifts in films have been observed by several groups.[87–89] Collier *et al.* have reviewed these interaction mechanisms[88] and Kagan *et al.* have proposed[89] that red-shifts occur due to energy migration *via* a process analogous to Forster transfer.

In the $Au@SiO_2$ nanoparticle films, the optical effects are due to controlled coupling of the nanoparticle dipoles. However, it is not always necessary for the core particles to couple to create novel optical effects. If the silica shell is grown to a thickness of several hundred nanometres, then there can be diffraction from the ordered colloid lattice. Such a lattice is commonly termed a photonic crystal or nanoparticle opal. Under optimal circumstances, there can also be inhibition of emission if the wavelength of the incident light corresponds to Bragg modes of such a photonic crystal.

Reasonably robust photonic crystals can be synthesized by derivatizing $CdS@SiO_2$ particles with TPM, and dispersing the particles in methyl methacrylate monomer. The TPM coated particles are slightly charged due to the presence of residual hydroxide ions on the silica surface.[59] This small charge renders the particles "soft", and determines the phase diagram. For TPM coated silica spheres, the fluid–solid phase transition has been observed at a particle volume fraction of $\phi = 0.194$, and the crystal–glass transition at $\phi = 0.224$.[90] The crystallization occurs all over the sample volume, so that small crystallites are formed, which can fill up the sample or co-exist with a fluid phase, depending on concentration, which also determines the crystallization rate. Photopolymerization of the ordered particles allows rigid films to be synthesized with the particles either ordered or randomly dispersed within the polymer matrix.[91] A photograph of a 1.5 cm square $CdS@SiO_2$ polymer glass film is shown in Fig. 16; it appears a transparent lemon-yellow colour. The film shows almost no light scattering because the PMMA matrix and silica shells have similar refractive indices. As nanoparticles crystallise to form photonic

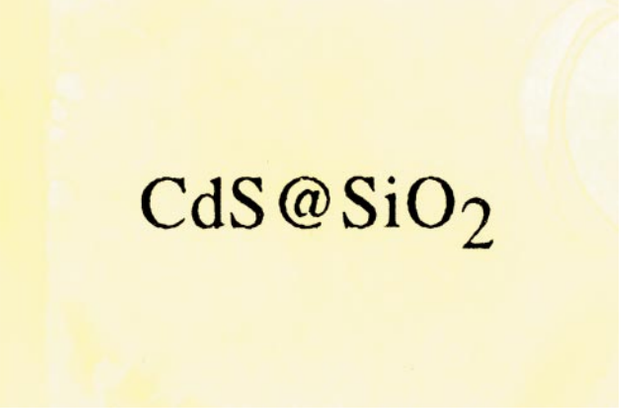

Fig. 16 Photograph of a macroscopic quantum dot lattice, synthesized from Q-$CdS@SiO_2$. Mean CdS diameter is 10 nm, silica shell thickness is 250 nm. Sample is 1.5 cm in length. The interparticle spacing can be tuned from 5 nm to 500 nm. Because of the index matching with PMMA, the silica shell matrix is almost completely transparent and text can be read through it.

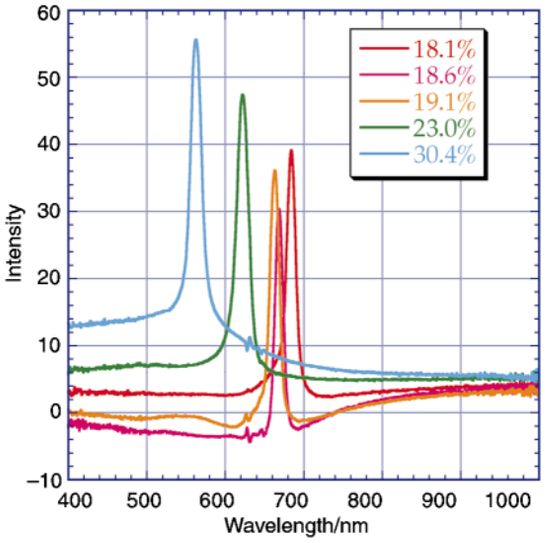

Fig. 17 Reflectance spectra obtained from concentrated $CdS@SiO_2$ colloids as a function of the volume fraction of particles. Coated particle diameter is 235 nm.[92]

crystals, the process can be monitored by observation of Bragg peaks in the reflectance specrum of the dense colloid. In Fig. 17, specular reflectance spectra of concentrated $CdS@SiO_2$ dispersions in EtOH are shown. As the volume fraction of the colloid particles is increased, the Bragg peak shifts to shorter wavelengths.

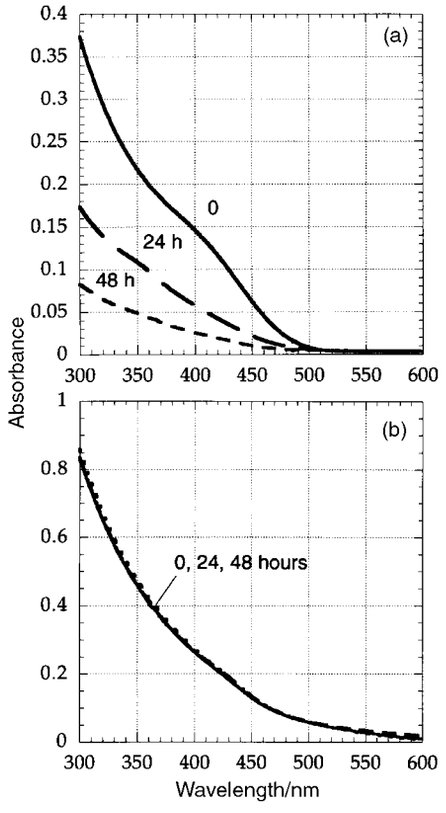

Fig. 18 Absorption spectra of colloidal CdS as a function of the time of irradiation in daylight (a) when stabilized by citrate and (b) after capping with silica. Solutions were air saturated. The curves refer to $t=0$, 24 hours and 48 hours irradiation.[93] The decrease in absorption over time is due to photodissolution *via* eqn. (24). Reprinted from *Chem. Phys. Lett.*, 1998, **286**, 497, with permission from Elsevier Science.

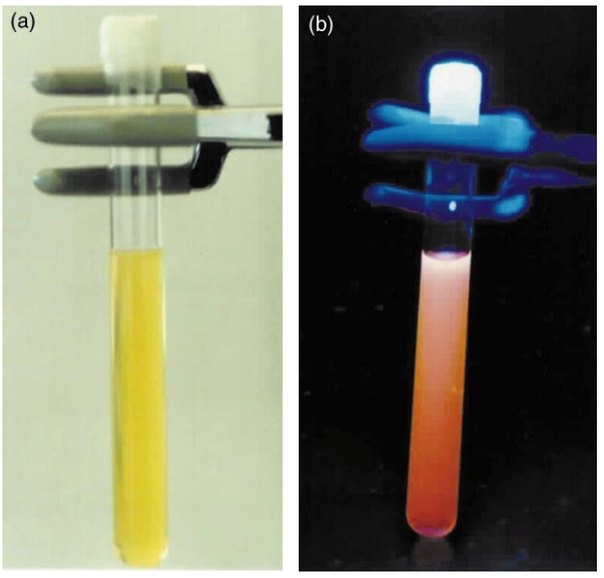

Fig. 19 Photograph of a sample of $CdS@SiO_2$ colloid in (a) visible light and (b) under UV irradiation showing intense red emission from trap states.

III.A Photochemical stabilization

A key feature of the silica shell is that it retards interactions with oxygen.[93] As a result, photochemical decomposition of semiconductor particles can be strongly reduced. In Fig. 18, the absorption spectra of uncoated CdS and $CdS@SiO_2$ colloids are shown as a function of the time of exposure to daylight. The sols are air-saturated. Photo-oxidation of CdS in aerated solution results in sulfate formation following scavenging of conduction electrons by adsorbed oxygen:[94,95]

$$CdS + O_2 \rightarrow Cd^{2+} + SO_4^{2-} \qquad (24)$$

In the absence of sufficient oxygen, direct electron–hole recombination dominates, and the material is photochemically stable. This provides a simple route towards the preparation of stable, fluorescently labelled silica. In Fig. 19, we show photographs of $CdS@SiO_2$ samples in visible light and under UV irradiation. The red fluorescence stems from sulfur vacancies. The silane coupling agent can enhance fluorescence yields by blocking surface sites, whilst the silica layer reduces quenching by oxygen. The degree of stability is affected by the porosity of the shell. The silica coated particles are at least 100 times more photochemically stable than the uncoated particles.

III.B Core–shell dissolution kinetics

Depending on the preparation conditions, the silica shell deposited retains a nano or mesoporous structure, which has been extensively investigated for larger silica particles by BET gas adsorption.[96] Cyanide ions will diffuse through the shell and dissolve the core metal in the case of silver or gold.[97]

The kinetics can be modelled provided a number of drastic simplifications are assumed. The solution to the diffusion equation was considered some 50 years ago by Barrer.[98,99] When a reactant is added at time zero, it is homogeneously distributed within the solvent, but has zero concentration within the shell and core. Assuming the rate of reaction with the core is very rapid, then diffusion through the shell is rate limiting. In general, the solution to the diffusion equation contains a transient and a steady state term. The transient term describes the build-up of the steady state concentration profile within the shell. A steady state is achieved when there is a linear concentration gradient within the shell layer, which acts to supply the core with fresh reagent at a constant rate. It is also

assumed that product build-up does not affect the reaction kinetics. With these limitations in place, the flux of reagent to the core of a single particle obeys:

$$J = 4\pi ab(a-b)C_o \times \left\{ \alpha - \frac{1}{6} - 2\pi^2 \sum_{n=1}^{n=\infty} \frac{(-1)^n}{n^2} \exp(-\alpha n^2 \pi^2) \right\} \quad (25)$$

Here C_o is the bulk concentration (mol cm^{-3}) of the reactant, D its diffusion coefficient within the pore, $\alpha = Dt/(b-a)^2$ is the normalized time, b is the shell thickness and a is the core radius. Comparison with the theory curves suggests the effective diffusion coefficient of cyanide ion within the silica shell is 10^{-10}–10^{-13} $cm^2\ s^{-1}$, a factor of 10^4–10^7 times slower than in bulk solution. A simple comparison of the effect of shell thickness can be made by monitoring gold dissolution in a colloid containing thick and thin shelled particles. TEM images presented in Fig. 20 clearly reveal that the thickly coated particles survive the cyanide etching for longer than the thinly coated ones.

III.C Quantum bubbles, single electron capacitors and new materials

The dissolution of the core to make quantum bubbles opens up a number of possibilities, and various groups have devised ways to engineer such materials.[100–107] These particles can make lattices and diffraction gratings through void diffraction. Note that the surface modes in such void lattices are discussed within the framework of the dipole model in ref. 77.[108] Another possibility is to use the core–shell matrix as a means to synthesize and stabilize materials difficult to generate in solution. An example of this is mercury. Mercury sols are virtually impossible to stabilize, though mixed amalgam sols of Hg–Ag can be prepared.[109] Above a critical Hg fraction, the particles coalesce. A different route is to prepare $HgS@SiO_2$ sols and reduce the HgS *in situ* to form Hg nanodroplets within the core. The process is not straightforward, because the Laplace pressure is so high that the mercury evaporates.[110] The sol is only stable at very low temperatures, close to the melting point of mercury.

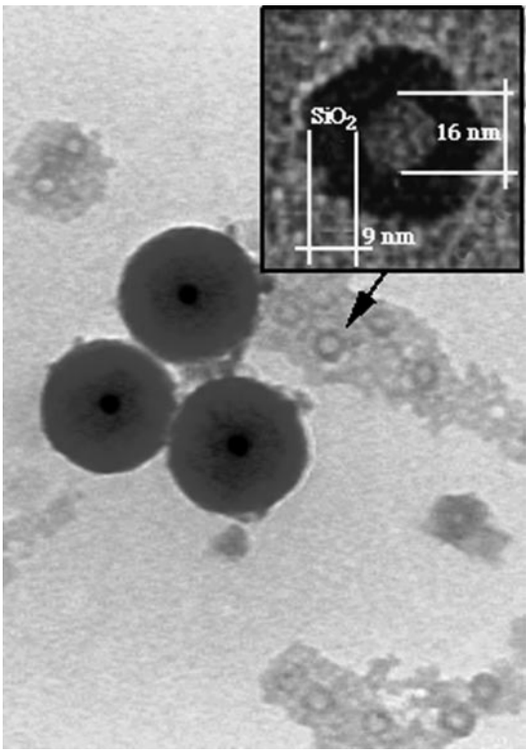

Fig. 20 TEM images of a colloid containing 15 nm gold particles that have been coated with 10 nm and 50 nm silica shells after exposure for 0.5 hours to KCN at pH 10.5. The particles with thicker shells survive longer than those with thinner shells.

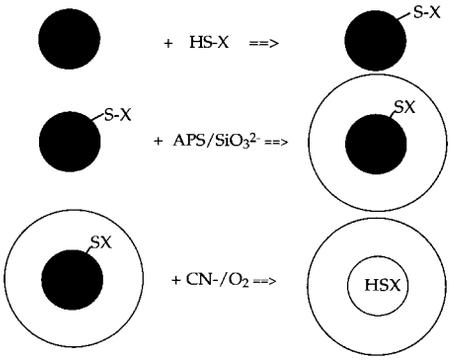

Fig. 21 Preparation of a quantum confined molecule using a mercaptan tag.[111,112] The tagged molecule is added at very low concentrations to a gold sol, then APS is added. Silica deposition coats the particle. Upon core dissolution with cyanide, the molecule is liberated within the quantum bubble.

Hollow spheres provide an alternative organized matrix for the study of quantum confinement on the spectroscopic properties of molecules. In Fig. 21, a simple method to create such an ensemble of confined molecules is shown, which has been successfully trialled by Meisel and colleagues.[111] The dye, alkane mercaptan or other probe molecule is adsorbed at submonolayer concentrations onto the gold surface together with APS. The particle is then coated with silica and etched by cyanide. This process is only weakly oxidizing, and will not affect the probe molecule. After dialysis to remove excess cyanide and $Au(CN)_2^-$, the probe is sterically trapped inside the shell.

Whilst $Core@SiO_2$ particles are ideal vehicles for constructing optical nanostructures, the lack of electrical conductivity of silica would appear to limit the use of these structures in electronic devices. However, for thicknesses of 1–2 nm, electrons can still tunnel through the shell. *I–V* curves for coated and uncoated (citrate stabilised) gold particles on a flame annealed Au(111) face are shown in Fig. 22.[112] The curve in the presence of the silica shell shifts to higher potentials,

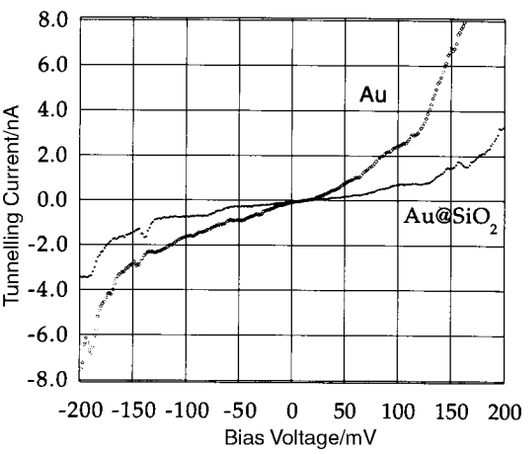

Fig. 22 *I–V* curves obtained by STM from citrate and silica capped gold particles. The gold core diameter is 15 nm. The silica shell thickness is 2–3 nm. The citrate layer is estimated to be 0.5 nm.[112] A commercial Pt tip was used. The particles were prepared on Au(111) surfaces annealed in a hydrogen flame. The current response shifts to higher potentials when the particle is coated, due to the need to tunnel through the silica shell.

reflecting the "overpotential" needed to drive tunnelling through the shell layer.

Conclusions

In this review, we have concentrated on the surface chemical aspects of $X@SiO_2$ structures, their formation and stabilization. In general, we have seen that the shell does not strongly perturb the core optical properties, but does enhance its lifetime as a nanoparticle by preventing both particle ripening and coagulation. Selective core etching allows the construction of further novel nanoparticle structures. We have tried to demonstrate that force measurements with the AFM may shed light on the role of capping agents and adsorbates on interparticle forces at the nanoparticle level. We have demonstrated some of the tunable optics that can be created with such core–shell structures, and finally we have discussed some new reaction geometries and materials currently under investigation.

Acknowledgements

T.U. is grateful for the receipt of an Australian Postgraduate Award; P.M. thanks the ARC for support, and L.M.L.M. acknowledges support from the Spanish Xunta de Galicia (Project No. PGIDT99PXI30104B) and from NATO Cooperation Grant CRG971167. We thank Miguel Correa-Duarte for providing the image shown in Fig. 19.

References

1 Derjaguin–Landau–Verwey–Overbeek laid the ground rules for colloid interactions. See ref. 37 for details.
2 L. P. Kouwenhoven and P. L. McEuen, in *Nanotechnology*, ed. G. Timp, Springer-Verlag, New York, 1999, ch. 13.
3 S. V. Gaponenko, *Optical Properties of Semiconductor Nanocrystals*, Cambridge University Press, UK, 1998.
4 (*a*) B. O'Regan and M. Grätzel, *Nature*, 1991, **353**, 737; (*b*) K. Fujihara, T. Ono and M. Matsumara, *J. Chem. Soc., Faraday Trans.*, 1998, **94**, 3705.
5 See *Photocatalysis, Fundamentals and Applications*, ed. N. Serpone and E. Pelizzetti, New York, 1989, for a comprehensive review of many of the ideas underlying removal of environmental pollutants through colloid photochemistry.
6 For example, C. Mirkin *et al.* use metal surface plasmon resonances to assay for single nucleotide base errors in *Nature*, 1996, **382**, 607, while $QD@SiO_2$ particles have been used as fluorescent labels by M. Bruchez, M. Moronne, P. Gin, S. Weiss and A. P. Alivisatos, *Science*, 1998, **281**, 2013 and by Chan and Nie, *ibid.*, p. 2016.
7 Y. Wang and N. Herron, *J. Phys. Chem.*, 1987, **91**, 257.
8 E. S. Smotkin, C. Lee, A. J. Bard, A. Campion, M. A. Fox, T. E. Mallook, S. E. Webber and J. M. White, *Chem. Phys. Lett.*, 1988, **152**, 265.
9 J. Fendler, *Chem. Mater.*, 1996, **8**, 1617.
10 F. Grieser, D. N. Furlong, D. Scoberg, I. Ichinose, N. Kimizuka and T. Kunitake, *J. Chem. Soc., Faraday Trans.*, 1992, **88**, 2207.
11 C. B. Murray, D. J. Norris and M. G. Bawendi, *J. Am. Chem. Soc.*, 1993, **115**, 8076.
12 J. Heath, *Science*, 1992, **258**, 1131.
13 M. D. Bentzon, J.van Wonterghem, S. Morup, A. Thölén and C. J. W. Koch, *Philos. Mag. B*, 1989, **60**, 169.
14 L. Motte, F. Billoudet and M. P. Pileni, *J. Phys. Chem.*, 1995, **99**, 16425.
15 (*a*) M. L. Steigerwald, A. P. Alivsatos, J. M. Gibson, T. D. Harris, R. Kortan, A. J. Muller, A. M. Thayer, T. M. Duncan, D. C. Douglass and L. E. Brus, *J. Am. Chem. Soc.*, 1988, **110**, 3046; (*b*) A. Kortan, R. Hull, R. Oplia, M. Bawendi, M. Steigerwald, P. Carroll and L. E. Brus, *J. Am. Chem. Soc.*, 1990, **112**, 1327.
16 General reviews of the use of microheterogeneous media for particle preparation are given in *Kinetics and Catalysis in Microheterogeneous Systems*, ed. M. Grätzel and K. Kalyansundaram, Marcel Dekker, New York, 1991, and in *Electrochemistry in Colloids and Dispersions*, ed. J. Texter and R. Mackay, VCH, New York, 1992.
17 V. Colvin, M. Schlamp and A. P. Alivisatos, *Nature*, 1994, **370**, 6488.
18 Y. Wang, A. Suna, W. Mahler and R. Kasowski, *J. Chem. Phys.*, 1987, **87**, 7315.
19 O. Micic, J. Sprague, Z. Lu and A. J. Nozik, *Appl. Phys. Lett.*, 1996, **68**, 3150.
20 A. I. Ekimov, Al. L. Efros and A. A. Onushchencko, *Solid State Commun.*, 1985, **56**, 921.
21 A. E. Hughes and S. C. Jain, *Adv. Phys.*, 1979, **28**, 717.
22 W. T. Doyle, *Phys. Rev.*, 1958, **111**, 1067.
23 U. Woggon, *Optical Properties of Semiconductor Quantum Dots, Springer Tracts in Modern Physics*, vol. 136, Springer, Berlin, 1997 discusses many of the original preparations in glasses.
24 L. Spanhel and M. A. Anderson, *J. Am. Chem. Soc.*, 1991, **113**, 2826.
25 (*a*) N. N. Parvathy, G. M. Pajonk and A. V. Rao, *Mater. Res. Bull.*, 1997, **32**, 397; (*b*) J. H. Adair, T. Kido, K. Harvey, J. Moon, J. Mecholsky, A. Morrone, D. Talham, M. Ludwig and L. Wang, *Mater. Sci. Eng. R*, 1998, **23**, 139.
26 O. Lev, Z. Wu, S. Bharathi, J. Gun, A. Modestov, L. Rabinovich and S. Sampath, *Chem. Mater.*, 1997, **6**, 2354.
27 A. Martino, S. A. Yamanaka, J. S. Kawola and D. A. Loy, *Chem. Mater.*, 1997, **9**, 423.
28 L. Spanhel, M. Haase, H. Weller and A. Henglein, *J. Am. Chem. Soc.*, 1987, **109**, 5649.
29 A. Henglein, *Top. Curr. Chem.*, 1988, **113**, 149.
30 *Fine Particles Science and Technology—From Micro to Nanoparticles*, ed. E. Pelizzetti, NATO ASI Series 3/12, Kluwer, Dordrecht, 1996.
31 *Nanoparticles, and Nanostructured Films: Preparation, Characterization and Utilization*, ed. J. Fendler, VCH-Wiley, Weinheim, 1998.
32 A review of particle synthesis and properties is given in A. Henglein, *Chem. Rev.*, 1989, **89**, 1861.
33 U. Resch, A. Eychmüller, M. Haase and H. Weller, *Langmuir*, 1992, **8**, 2215.
34 A. Henglein, A. Fojtik and H. Weller, *Ber. Bunsen-Ges. Phys. Chem.*, 1987, **91**, 447.
35 H. Weller, U. Koch and A. Henglein, *Ber. Bunsen-Ges. Phys. Chem.*, 1984, **88**, 969.
36 A. C. Templeton, S. Chen, S. Gross and R. W. Murray, *Langmuir*, 1999, **15**, 66.
37 R. J. Hunter, *Foundations of Colloid Science*, Oxford University Press, New York, 1989, vol. 1.
38 J. Israelachvili, *Intermolecular and Surface Forces*, 2nd edn., Academic Press, San Diego, CA, 1992.
39 G. R. Wiese and T. W. Healy, *Trans. Faraday Soc.*, 1970, **66**, 490.
40 P. Hiemenz, *Principles of Colloid and Surface Chemistry*, Marcel Dekker, New York, 1986.
41 K. T. Miller and C. F. Zukoski, in *Semiconductor Nanoparticles—Physical, Chemical and Catalytic Aspects*, ed. D. Meisel and P. Kamat, Elsevier, Amsterdam, 1997, pp. 23–57.
42 J. N. Israelachvili, *Proc. R. Soc. London A*, 1972, **331**, 39.
43 W. A. Ducker, T. Senden and R. M. Pashley, *Langmuir*, 1993, **9**, 2232.
44 S. Biggs, P. Mulvaney, C. F. Zukoski and F. Grieser, *J. Am. Chem. Soc.*, 1994, **116**, 9150.
45 W. A. Ducker, T. J. Senden and R. M. Pashley, *Langmuir*, 1992, **8**, 1831.
46 S. Biggs and P. Mulvaney, *J. Chem. Phys.*, 1994, **100**, 8501.
47 Ya. Rabinovich and N. V. Churaev, *Kolloidn. Zh.*, 1990, **52**, 256.
48 B. V. Enüstün and J. Turkevich, *J. Am. Chem. Soc.*, 1963, **85**, 3317.
49 K. Hu and A. J. Bard, *Langmuir*, 1997, **13**, 5114.
50 V. Kane and P. Mulvaney, *Langmuir*, 1998, **14**, 3303.
51 R. K. Iler, *The Chemistry of Silica*, Wiley, New York, 1979.
52 L. Allen and E. Matijevic, *J. Colloid Interface Sci.*, 1969, **31**, 287; 1970, **33**, 420.
53 R. K. Iler, *The Chemistry of Silica*, Wiley, New York, 1979.
54 D. E. Yates and T. W. Healy, *J. Colloid Interface Sci.*, 1976, **55**, 9.
55 D. N. Furlong, P. A. Freeman and A. C. Lau, *J. Colloid Interface Sci.*, 1981, **80**, 21.
56 P. Hartley, I. Larson and P. J. Scales, *Langmuir*, 1997, **13**, 2207.
57 L. M. Liz-Marzán and P. Mulvaney, *New J. Chem.*, 1998, **22**, 1285.
58 A. K. van Helden, J. W. Jansen and A. Vrij, *J. Colloid Interface Sci.*, 1984, **81**, 354.
59 A. P. Philipse and A. Vrij, *J. Colloid Interface Sci.*, 1989, **128**, 121.
60 R. D. Badley, W. T. Ford, F. J. McEnroe and R. A. Assink, *Langmuir*, 1990, **6**, 792.

61 (*a*) M. Ohmori and E. Matijévic, *J. Colloid Interface Sci.*, 1993, **160**, 288; (*b*) T. Ishikara and E. Matijévic, *Langmuir*, 1988, **4**, 26; (*c*) H. Giesche and E. Matijévic, *J. Mater. Res.*, 1994, **9**, 436.
62 L. M. Liz-Marzán and A. P. Philipse, *J. Colloid Interface Sci.*, 1995, **176**, 459.
63 L. M. Liz-Marzán, M. Giersig and P. Mulvaney, *Chem. Commun.*, 1996, 731.
64 T. Ung, L. M. Liz-Marzán and P. Mulvaney, *Langmuir*, 1998, **14**, 3740.
65 I. Pastoriza-Santos and L. M. Liz-Marzán, *Langmuir*, 1999, **15**, 948.
66 P. Mulvaney, M. Giersig and A. Henglein, *J. Phys. Chem.*, 1992, **96**, 10419.
67 R. H. Doremus, *J. Chem. Phys.*, 1965, **42**, 414.
68 I. N. Shklyareskii, E. Anachkova and G. S. Blyashenko, *Opt. Spectrosc. (USSR)*, 1977, **43**, 427.
69 G. C. Papavassiliou, *Z. Phys. Chem. (Leipzig)*, 1976, **257**, 241.
70 S. Underwood and P. Mulvaney, *Langmuir*, 1994, **10**, 3427.
71 P. Mulvaney, in *Semiconductor Nanoclusters—Physical, Chemical and Catalytic Aspects*, ed. D. Meisel and P. Kamat, Elsevier, Amsterdam, 1997, pp. 99–125.
72 P. Mulvaney, *Langmuir*, 1996, **12**, 788.
73 G. C. Papavassiliou, *J. Phys. F: Met. Phys.*, 1976, **6**, L103.
74 P. Mulvaney, M. Giersig and A. Henglein, *J. Phys. Chem.*, 1993, **97**, 7061.
75 C. de Cointet, J. Khatouri, M. Mostafavi and J. Belloni, *J. Phys. Chem.*, 1997, **18**, 3517.
76 M. Treguer, C. de Cointet, H. Remita, J. Khatouri, M. Mostafavi, J. Amblard, J. Belloni and R. de Keyzer, *J. Phys. Chem.*, 1998, **102**, 4310.
77 C. F. Bohren and D. Huffman, *Absorption and Scattering of Light by Small Particles*, Wiley, New York, 1983.
78 L. M. Liz-Marzán, M. Giersig and P. Mulvaney, *Langmuir*, 1996, **12**, 4329.
79 AgI dielectric data were taken from L. D. Bedikyan, V. K. Miloslavskii and L. A. Ageev, *Opt. Spectrosc. (USSR)*, 1979, **47**, 225.
80 P. Mulvaney, *Colloids Surf. A*, 1993, **81**, 231.
81 L. M. Liz-Marzán and P. Mulvaney, *Recent Res. Dev. Phys. Chem.*, 1998, **2**, 1.
82 J. C. Maxwell-Garnett, *Philos. Trans. R. Soc. London*, 1904, **203**, 385; 1906, **205**, 237.
83 D. A. Bruggeman, *Ann. Phys. (Leipzig)*, 1935, **24**, 634.
84 C. G. Granqvist and O. Hunderi, *Z. Phys. B*, 1978, **30**, 47.
85 T. Ung, L. M. Liz-Marzán and P. Mulvaney, *J. Phys. Chem.*, submitted.
86 N. A. Kotov, I. Dékány and J. Fendler, *J. Phys. Chem.*, 1995, **99**, 13065.
87 J. J. Shiang, J. R. Heath, C. P. Collier and R. J. Saykally, *J. Phys. Chem. B*, 1998, **102**, 3425.
88 C. P. Collier, T. Vossmeyer and J. R. Heath, *Annu. Rev. Phys. Chem.*, 1998, **49**, 371.
89 C. R. Kagan, C. B. Murray, M. Nirmal and M. G. Bawendi, *Phys. Rev. Lett.*, 1996, **76**, 1517.
90 J. K. G. Dhont, C. Smits and H. N. W. Lekkerkerker, *J. Colloid Interface Sci.*, 1992, **152**, 386.
91 H. Sunkara, J. M. Jethmalani and W. T. Ford, *ACS Polym. Mater. Sci. Eng. Preprints*, 1994, **74**, 274.
92 M. Alejandro-Arellano, *Masters Thesis*, University of Vigo.
93 M. A. Correa-Duarte, M. Giersig and L. M. Liz-Marzán, *Chem. Phys. Lett*, 1998, **286**, 497.
94 D. Meissner, R. Memming, L. Shuben, S Yesodhara and M. Grätzel, *Ber. Bunsen-Ges. Phys. Chem.*, 1985, **89**, 21.
95 A. Henglein, *Ber. Bunsen-Ges. Phys. Chem.*, 1982, **86**, 301.
96 A. van Blaaderen and A. Vrij, *J. Colloid Interface Sci.*, 1993, **156**, 1.
97 M. Giersig, T. Ung, L. M. Liz-Marzán and P. Mulvaney, *Adv. Mater.*, 1997, **9**, 570.
98 R. M. Barrer, *Philos. Mag.*, 1944, **35**, 802.
99 J. Crank, *The Mathematics of Diffusion*, 2nd edn., Clarendon Press, Oxford, 1975.
100 F. Caruso, R. A. Caruso and H. Möhwald, *Science*, 1998, **282**, 1111.
101 A. Imhof and D. J. Pine, *Nature*, 1997, **389**, 948.
102 A. Imhof and D. J. Pine, *Adv. Mater.*, 1998, **10**, 697.
103 B. T. Holland, C. F. Blanford and A. Stein, *Science*, 1998, **281**, 538.
104 J. E. G. J. Wijnhoven and W. L. Vos, *Science*, 1998, **281**, 802.
105 S. I. Matsushita, T. Miwa, D. A. Tryk and A. Fujishima, *Langmuir*, 1998, **14**, 6441.
106 S. M. Marinakos, D. A. Shultz and D. L. Feldheim, *Adv. Mater.*, 1999, **11**, 34.
107 T. K. Jain, I. Roy, T. K. De and A. Maitra, *J. Am. Chem. Soc.*, 1998, **120**, 11092.
108 Ref. 77, p. 330.
109 A. Henglein and C. Brancewicz, *Chem. Mater.*, 1997, **9**, 2164.
110 T. Ung and P. Mulvaney, unpublished data.
111 O. V. Makarova, A. E. Ostafin, H. Miyoshi, J. R. Norris and D. Meisel, *J. Phys. Chem. B*, 1999, **103**, 9080.
112 S.-T. Yau, P. Mulvaney, W. Xu and G. M. Spinks, *Phys. Rev. B*, 1998, **57**, R15124.